

Lateral load effects on tall shear wall structures of different height

*Original*

Lateral load effects on tall shear wall structures of different height / Carpinteri, Alberto; Corrado, Mauro; Lacidogna, Giuseppe; Cammarano, Sandro. - In: STRUCTURAL ENGINEERING AND MECHANICS. - ISSN 1225-4568. - STAMPA. - 41:3(2012), pp. 313-337. [10.12989/sem.2012.41.3.313]

*Availability:*

This version is available at: 11583/2485234 since: 2015-11-26T10:31:34Z

*Publisher:*

Techno Press

*Published*

DOI:10.12989/sem.2012.41.3.313

*Terms of use:*

This article is made available under terms and conditions as specified in the corresponding bibliographic description in the repository

*Publisher copyright*

(Article begins on next page)

## Lateral load effects on tall shear wall structures of different height<sup>†</sup>

Alberto Carpinteri, Mauro Corrado, Giuseppe Lacidogna\* and Sandro Cammarano

*Department of Structural and Geotechnical Engineering, Politecnico di Torino, Torino, Italy*

*(Received July 23, 2010, Revised December 22, 2011, Accepted January 3, 2012)*

**Abstract.** A three-dimensional formulation is proposed to analyze the lateral loading distribution of external actions in high-rise buildings. The method is extended to encompass any combination of bracings, including bracings with open thin-walled cross-sections, which are analyzed in the framework of Timoshenko-Vlasov's theory of sectorial areas. More in detail, the proposed unified approach is a tool for the preliminary stages of structural design. It considers infinitely rigid floors in their own planes, and allows to better understand stress and strain distributions in the different bearing elements if compared to a finite element analysis. Numerical examples, describing the structural response of tall buildings characterized by bracings with different cross-section and height, show the effectiveness and flexibility of the proposed method. The accuracy of the results is investigated by a comparison with finite element solutions, in which the bracings are modelled as three-dimensional structures by means of shell elements.

**Keywords:** structural behaviour; modelling methods; tall buildings; lateral loading distribution; thin-walled cross-section; Timoshenko-Vlasov's theory; finite element method

---

### 1. Introduction

From the structural viewpoint, tall building means a multi-storey construction in which the effects of horizontal actions and the need to limit the relative displacements take on primary importance (Taranath 1988, 2005). A profound understanding of the force flow in these complex structural systems is often very difficult, and a huge commitment in terms of design, technology and economic resources is required. While in the design of low-rise structures the strength requirement is the dominant factor, with increasing height, the importance of the rigidity and stability requirements to be met to counter wind and earthquake actions grows until they become the prevailing design factors (note that the latest skyscrapers rise to over 800 m, the tallest of all being "Burj Khalifa Dubai" tower in Dubai, 828 m high). For this reason, the traditional solutions providing for load-bearing main and secondary parts tend to be forsaken in favour of a global approach, whereby the structure is conceived in a unitary fashion, i.e., as a single cantilever beam or a system of cantilevers projecting out from the foundations. At any rate, the key issue in structural design continues to be the choice of an appropriate design model, that is able to reproduce faithfully

---

\*Corresponding author, Associate Professor, E-mail: giuseppe.lacidogna@polito.it

<sup>†</sup>The present contribution is dedicated to the memory of the late Professor Michele Capurso, in the 25th Anniversary of his death.

the actual conditions of a structure.

Concerning the model choice, over the last three decades, it seems that a large part of the engineering community has followed a path towards the use of Finite Element (FE) models also in the early stage of design. These models can take into account any level of detail, since they model the structure in its entirety. However, as remarked by several Authors (Howson 2006, Steenbergen and Blaauwendraad 2007), they have their drawbacks. Even using powerful computers, the modelling is usually very demanding and the lengthy and time-consuming procedure of handling all the data can always be a source for errors. In addition and most importantly, because of the complexity of the results, they are difficult to be interpreted and it is not easy to understand from FE simulations which structural parameters govern the response of the structure and the interaction among its elements, or clearly to identify the paths of force flow in the structure. In a sense, the importance of the key structural elements is somehow concealed behind the great number of input and output data. As remarked by Howson (2006), the use of FE models is not in question for the detailed design and analysis, but the development of such a model at an early stage in a design process can be not only time consuming but also unproductive, if used during a period of rapid evolution of the concept.

On the other hand, the use of analytical models seems to set a reverse trend. Simplified procedures relying on carefully chosen approximations, in fact, cannot be renounced to fully understand the complex behaviour of high-rise structures. A simplified global model, in fact, can offer a number of potential advantages: data preparation and analysis is definitely faster; the modelling procedures are likely to be simpler and more transparent, thus less prone to be a potential source of errors; the accuracy, although not as high as in FE simulations, is sufficient for the preliminary design stage. Most importantly, the use of this kind of procedures offers a clear picture of the structural behaviour, allowing to gain insight into the key structural parameters governing the tall building behaviour.

The earliest models, developed in the 1960's and 1970's, addressed the case of shear-wall versus frame interaction; among them we could cite the approaches by Khan and Sbarounis (1964), Coull and Irwin (1972), Heidebrecht and Stafford Smith (1973), Rutenberg and Heidebrecht (1975), Mortelmans *et al.* (1981). In all these models, however, only one degree of freedom per storey is considered, and the torsional problem is treated separately.

Most of the models for the analysis of coupled shear wall structures are based on the continuum medium technique. The principle of the method is to replace the effect of individual beams or slabs, which interconnect the walls at each floor, by continuously distributed shear forces, that concur to stiffen the structural behaviour. In this framework, the whole structure is idealized as a single shear-flexural cantilever. This method was proposed in the pioneering papers by Rosman (1964, 1965, 1966), Beck *et al.* (1968), Beck and Schäfer (1969). According to the development of the tall building typologies, these models were devoted to framed wall structures, as in the papers by Stamato and Mancini (1973), Gluck and Krauss (1973), as well as to framed-tube structures, as in the papers by Khan (1974), Coull and Bose (1977) among others. The continuum medium technique has then been extended to other structural typologies (Stafford Smith and Coull 1991, Hoenderkamp and Snijder 2000, Lee *et al.* 2008). Moreover, the effects of rigid beams or slabs on the distribution of the forces between shear walls have been further investigated by Fischer and Kasal (2009). In their analysis the stiffness variation of resistant walls, due to imperfections or openings, is taken into account by means of reduction factors.

A different research direction, derived from aerospace engineering, is that based on subdivision of

the structure into substructures; it is somehow in between the simplified models and the FE approach, since the substructures are used to formulate super-elements, either by condensation or by analytical procedures with exact solutions. Among others, we could cite the papers by Leung (1985), Leung and Wong (1988), Wong and Lau (1989), as well as the so-called finite storey method (FSM) by Pekau *et al.* (1995, 1996). More recent works include, among others, the approaches presented by Kim and Lee (2003), Steenbergen and Blaauwendraad (2007).

The main problem with all these simplified models is the lack of generality, since the same formulation often cannot be used to analyse buildings with different underlying structural typologies. In addition, several of them consider two-dimensional plane structures. However, not all buildings can be modelled as plane structures, especially in the case of very complex shapes. With the aim at acquiring insight into the effects of the stability element typologies and arrangements in tall buildings within a unified framework, and the capability of modelling complex structures and different typologies, in this paper we propose a three-dimensional formulation based on the work by Carpinteri and Carpinteri (1985). The formulation is extended to encompass any combination of bracings, including bracings with open thin-walled cross-sections, which are analyzed in the framework of Timoshenko-Vlasov's theory (Timoshenko 1936, Vlasov 1961) of sectorial areas, and according to the approach by Capurso (1981), as recently proposed by Carpinteri *et al.* (2010). Numerical examples, investigating the structural response of tall buildings characterized by bracings with different cross-section and height, show the effectiveness and flexibility of the proposed approach. Furthermore, the accuracy of the results is investigated by a comparison with FE solutions, in which the bracings are modelled as three-dimensional structures by means of shell elements.

## 2. Analytical formulation

The general formulation of the problem of the external lateral loading distribution between the bracings of a three-dimensional civil structure, originally presented by Carpinteri and Carpinteri (1985), will be revisited in this section. The structure is idealized as consisting of  $M$  bracings interconnected through floors undeformable in their planes and the axial deformation of bracings is not considered. With these hypotheses, the floor movement can be expressed by three generalized coordinates: the two translations,  $\xi$  and  $\eta$ , in X- and Y-direction of the global coordinate system origin (Fig. 1) and the floor rotation,  $\vartheta$ . If  $N$  is the number of storeys, the external load will be represented by a  $3N$ -vector  $\mathbf{f}$ , whose elements are three elementary loads for each floor and, more exactly, two shear forces,  $p_x$  and  $p_y$ , and the torsional moment,  $m_z$ . In the same way, the internal loading transmitted to the  $i$ -th element will be represented by a  $3N$ -vector  $\mathbf{f}_i$  and obtained from the preceding  $\mathbf{f}$  through a pre-multiplication by a distribution matrix. Let  $\mathbf{p}_i$  be the  $2N$ -vector representing the shear-loadings  $p_x$  and  $p_y$ , on the  $i$ -th element in the global coordinate system XY (Figs. 1 and 2), and  $\mathbf{m}_i$  the  $N$ -vector representing the torsional moments, so that

$$\mathbf{f}_i = \begin{Bmatrix} \mathbf{p}_i \\ \mathbf{m}_i \end{Bmatrix} \quad (1)$$

The internal loadings  $\mathbf{f}_i$  transmitted to the  $i$ -th bracing and related to the global coordinate system XY are connected with the same loadings  $\mathbf{f}_i^*$  related to the local coordinate system  $X_i^*Y_i^*$  (the origin

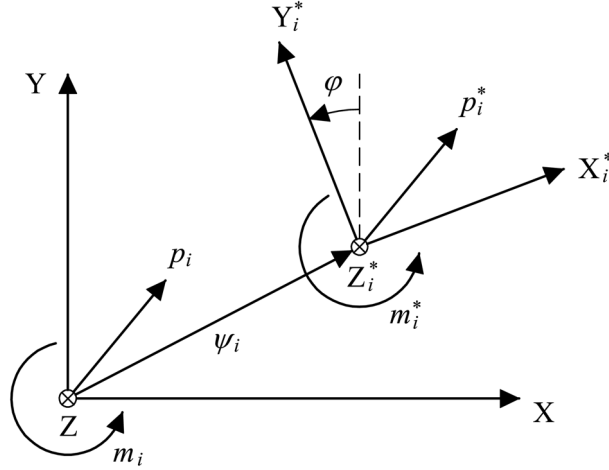


Fig. 1 Global and local coordinate systems. The Z-axis completes the right-handed global system XYZ and Zi\* completes the right-handed local system Xi\* Yi\* Zi\*.

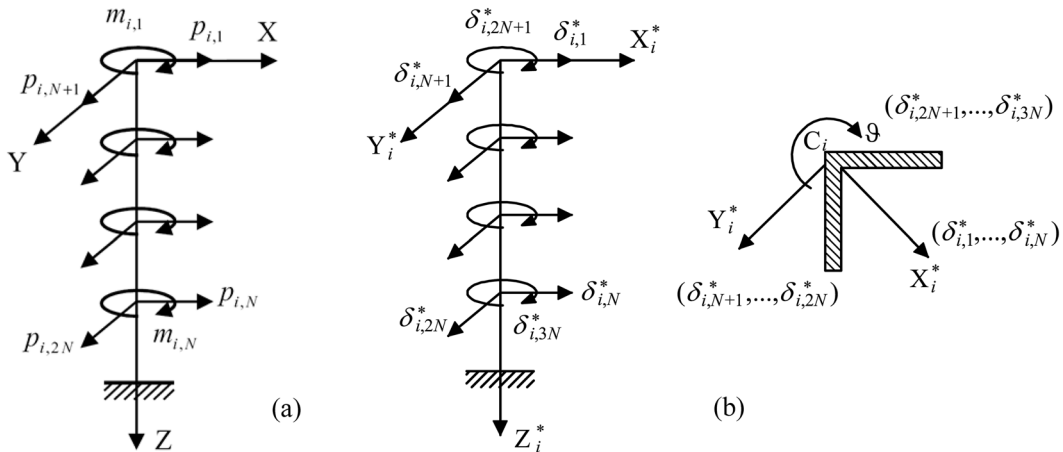


Fig. 2 Internal loadings  $f_i$  (transmitted to the  $i$ -th bracing) in the global coordinate system (a); degrees of freedom of the  $i$ -th bracing in the local coordinate system  $X_i^*Y_i^*Z_i^*$ , axonometry and top view (b). Note that the highest floor is indicated with 1 and the lowest with  $N$ .

of this system is in the shear centre  $C_i$  and the  $X_i^*Y_i^*$  axes are the principal ones, see Figs. 1 and 2(b)):

$$\mathbf{p}_i^* = \mathbf{N}_i \mathbf{p}_i \tag{2}$$

$$m_i^* = m_i - \boldsymbol{\psi}_i \times \mathbf{p}_i \cdot \mathbf{u}_z \tag{3}$$

where the superscript  $*$  is used to indicate the loadings in the local coordinate system  $X_i^*Y_i^*$ ,  $\mathbf{N}_i$  is

the orthogonal matrix of transformation from the system  $XY$  to the system  $X_i^*Y_i^*$ ,  $\boldsymbol{\psi}_i$  is the coordinate-vector of the origin of the local system  $X_i^*Y_i^*$  in the global one  $XY$ ,  $\mathbf{u}_z$  is the unit vector in the  $Z$ -direction (note that  $\boldsymbol{\psi}_i \times \mathbf{p}_i \cdot \mathbf{u}_z$  is a scalar triple product). The orthogonal matrix  $\mathbf{N}_i$  is represented as

$$\mathbf{N}_i = \begin{bmatrix} \cos \varphi & \sin \varphi \\ -\sin \varphi & \cos \varphi \end{bmatrix} \quad (4)$$

where each element represents a diagonal  $N \times N$ -matrix and  $\varphi$  is the angle between the  $Y_i^*$ -axis and the  $Y$ -axis (Fig. 1).

Eqs. (2) and (3) may be represented in the matrix form

$$\mathbf{f}_i^* = \mathbf{A}_i \mathbf{f}_i \quad (5)$$

where

$$\mathbf{A}_i = \begin{bmatrix} \mathbf{N}_i & \mathbf{0} \\ -\mathbf{C}_i^T & \mathbf{I} \end{bmatrix} \quad (6)$$

$\mathbf{I}$  is the identity matrix,  $\mathbf{0}$  the null matrix and the  $N \times 2N$ -matrix  $\mathbf{C}_i^T$  is defined as

$$\mathbf{C}_i^T = [-y_i \ x_i] \quad (7)$$

where each element is a diagonal  $N \times N$ -matrix and  $(x_i, y_i)$  are the components of vector  $\boldsymbol{\psi}_i$ .

The displacements  $\delta_i$  in the global coordinate system  $XY$  are then connected with the displacements  $\delta_i^*$  in the local system  $X_i^*Y_i^*$

$$\delta_i^* = \mathbf{B}_i \delta_i \quad (8)$$

where

$$\mathbf{B}_i = \begin{bmatrix} \mathbf{N}_i & \mathbf{0} \\ \mathbf{0} & \mathbf{I} \end{bmatrix} \quad (9)$$

The internal loadings  $\mathbf{f}_i^*$  are connected with the displacements  $\delta_i^*$  through the relation

$$\mathbf{f}_i^* = \mathbf{K}_i^* \delta_i^* \quad (10)$$

where  $\mathbf{K}_i^*$  is the condensed stiffness matrix in the local system. Recalling Eqs. (5) and (8), we get

$$\mathbf{A}_i \mathbf{f}_i = \mathbf{K}_i^* \mathbf{B}_i \delta_i \quad (11)$$

Pre-multiplying both the members by the inverse of  $\mathbf{A}_i$

$$\mathbf{f}_i = (\mathbf{A}_i^{-1} \mathbf{K}_i^* \mathbf{B}_i) \delta_i \quad (12)$$

it follows that the stiffness matrix in the global system for the  $i$ -th bracing is

$$\mathbf{K}_i = \mathbf{A}_i^{-1} \mathbf{K}_i^* \mathbf{B}_i \quad (13)$$

where

$$\mathbf{K}_i^* = \begin{bmatrix} \mathbf{K}_{pi}^* & \mathbf{0} \\ \mathbf{0} & \mathbf{K}_{mi}^* \end{bmatrix} \quad (14)$$

The displacement  $3N$ -vector  $\delta_i$  of the  $i$ -th element is connected with the displacement  $3N$ -vector  $\delta$  of the rigid floors by the relation

$$\delta_i = \mathbf{T}_i \delta \quad (15)$$

where the transformation  $3N \times 3N$ -matrix  $\mathbf{T}_i$  is

$$\mathbf{T}_i = \begin{bmatrix} \mathbf{I} & \mathbf{C}_i \\ \mathbf{0} & \mathbf{I} \end{bmatrix} \quad (16)$$

and the  $2N \times N$ -matrix  $\mathbf{C}_i$  is defined in Eq. (7).

Eq. (12) can be rewritten

$$\mathbf{f}_i = \mathbf{K}_i \mathbf{T}_i \delta = \overline{\mathbf{K}}_i \delta \quad (17)$$

where  $\overline{\mathbf{K}}_i = \mathbf{K}_i \mathbf{T}_i$  is the stiffness of the  $i$ -th element with respect to the floor displacements. For the global equilibrium we have

$$\sum_{i=1}^M \mathbf{f}_i = \sum_{i=1}^M \overline{\mathbf{K}}_i \delta \quad (18)$$

$$\mathbf{f} = \overline{\mathbf{K}} \delta \quad (19)$$

where  $\overline{\mathbf{K}}$  is the global stiffness matrix of the system. Recalling Eqs. (17) and (19), we get

$$\delta = \overline{\mathbf{K}}_i^{-1} \mathbf{f}_i = \overline{\mathbf{K}}^{-1} \mathbf{f} \quad (20)$$

and then

$$\mathbf{f}_i = \overline{\mathbf{K}}_i \overline{\mathbf{K}}^{-1} \mathbf{f} \quad (21)$$

Eq. (21) solves the problem of the external loading distribution between the resistant elements of a building. It is formally analogous to the equation for the distribution of a force between different in-parallel resistant elements in a plane problem. In fact, the distribution matrix  $\overline{\mathbf{K}}_i \overline{\mathbf{K}}^{-1}$  is the product of the partial stiffness matrix by the inverse of the total stiffness matrix, as well as in the plane problem the distribution factor is the product of the partial stiffness by the inverse of the total stiffness. The sum of the distribution matrices is equal to the unit matrix. Details on the condensation procedure for the computation of the stiffness matrices according to the de Saint Venant theory of beams with closed cross-section can be found in Humar and Kandhoker (1980). On the other hand, it can be observed that the above presented formulation is general and can be extended to encompass different kind of structural elements. To this aim, a procedure to compute the stiffness matrices for open thin-walled cross-sections is proposed in the next section.

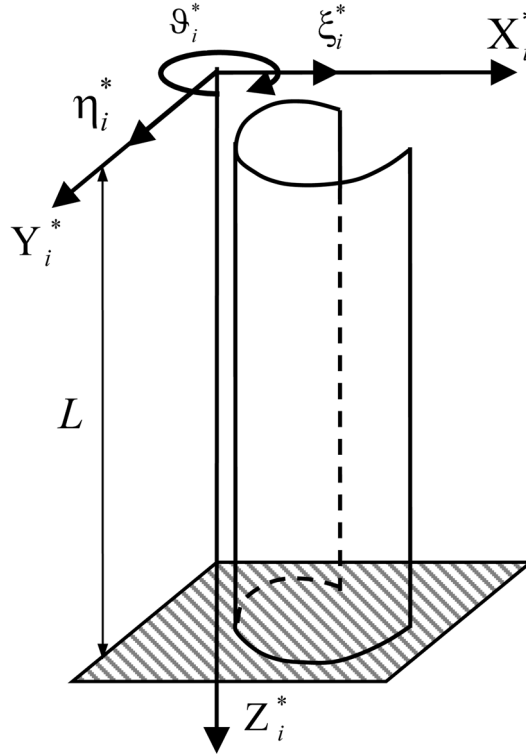


Fig. 3 Capurso's approach (1981): displacements of the  $i$ -th open thin-walled bracing in the local coordinate system  $X_i^*Y_i^*Z_i^*$

### 3. Stiffness matrix of open thin-walled bracings

The behaviour of open thin-walled cross-sections is treated according to the Timoshenko-Vlasov torsion theory of beams characterized by the presence of the warping stiffness (Timoshenko 1936, Vlasov 1961). With reference to Figs. 1 and 3, let us consider a generic beam in its local system  $X_i^*Y_i^*Z_i^*$ . If the beam sections are undeformable in their planes, the section movements can be expressed by three displacements: the two translations  $\xi_i^*$  and  $\eta_i^*$  (in  $X_i^*$ - and  $Y_i^*$ -direction of the local coordinate system origin, see Fig. 2) and the floor rotation  $\vartheta_i^*$ . Under the customary assumption that the lateral edges of the beam are free from shear forces and the external loads are distributed transverse flexural loads,  $p_x(z)$  and  $p_y(z)$ , and torsional moments,  $m_z(z)$ , only, so that the longitudinal force  $N$  at any value of  $z$  is zero, according to the analytical approach by Capurso (1981), it can be shown that the following relations, written in synthetic matrix form, hold

$$\mathbf{m}_i^*(z) = -E\mathbf{J}_i\delta_i^{*''}(z) \quad (22)$$

$$\mathbf{t}_i^*(z) = -E\mathbf{J}_i\delta_i^{*'''}(z) \quad (23)$$

if we introduce the following vectors



$$\delta_i^* = \begin{Bmatrix} \xi_i^* \\ \eta_i^* \\ \mathcal{G}_i^* \end{Bmatrix}, \quad \mathbf{m}_i^* = \begin{Bmatrix} M_{i,y}^* \\ M_{i,x}^* \\ B_i^* \end{Bmatrix}, \quad \mathbf{t}_i^* = \begin{Bmatrix} T_{i,x}^* \\ T_{i,y}^* \\ M_{i,z}^* \end{Bmatrix} \quad (24)$$

and the matrix of inertia

$$\mathbf{J}_i = \begin{bmatrix} J_{yy} & J_{yx} & J_{y\omega} \\ J_{xy} & J_{xx} & J_{x\omega} \\ J_{\omega y} & J_{\omega x} & J_{\omega\omega} \end{bmatrix} \quad (25)$$

where  $M_x(z)$  and  $M_y(z)$  are the functions representing the bending moments along the bracing,  $B(z)$  is the bimoment (Timoshenko 1936, Vlasov 1961),  $T_x(z)$  and  $T_y(z)$  are the shear forces,  $M_z(z)$  is the torsional moment,  $E$  is the Young's modulus, and the apex ' ' corresponds to derivation with respect to the axial coordinate  $z$ .  $J_{xx}$ ,  $J_{xy}$  and  $J_{yy}$  are the second order moments of inertia referred to the barycentre of the cross-section.  $J_{\omega\omega}$  is the sectorial moment of inertia, and  $J_{x\omega}$  and  $J_{y\omega}$  are the sectorial products of inertia referred to the shear centre of the cross-section.

By further deriving Eq. (23) we get

$$\mathbf{f}_i^*(z) = E\mathbf{J}_i\delta_i^{*IV}(z) \quad (26)$$

where  $\mathbf{f}_i^*(z)$  is a 3-vector containing the external load distributions.

Since the matrix of inertia  $\mathbf{J}_i$  is symmetric and positive definite, except for some anomalous cases (detailed by Capurso 1981), Eq. (26) can be inverted and the components of vector  $\delta_i^{*IV}$  can be computed

$$\delta_i^{*IV}(z) = \frac{1}{E}\mathbf{J}_i^{-1}\mathbf{f}_i^*(z) \quad (27)$$

Considering Eq. (27) and integrating it with the appropriate boundary conditions, it is possible to obtain the relationship between the applied loads and the displacements, i.e., the stiffness matrix in the local system to be used in the general formulation proposed in the previous section. When the external loads are concentrated forces at each floor level, instead of distributed loads, Eq. (27) is no longer valid at the floor level, where discontinuities are present. As a result,  $N$  equations can be written, one for each field delimited by a couple of subsequent storeys, having the following form

$$\delta_i^{*IV}(z) = 0 \quad (28)$$

In this case, the integration process should be performed by integrating the  $N$  equations like Eq. (28), with the boundary condition and the  $(N-1)$  conditions of continuity between adjacent fields. More in detail, the boundary condition for the first step of integration is

$$\delta_i^{*'''(0)} = -\frac{1}{E}\mathbf{J}_i^{-1}\mathbf{f}_i^*(0) \quad (29)$$

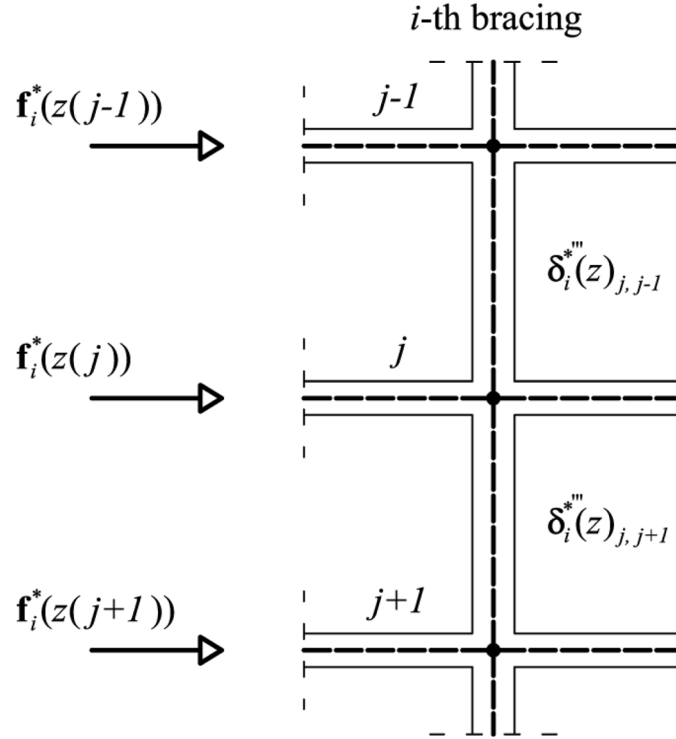


Fig. 4 Scheme for the introduction of the applied loads in the integration steps

On the other hand, the conditions of continuity permit to introduce the applied loads, as follows (see Fig. 4)

$$\delta_i^{*'''}(z(j))_{j,j+1} = \delta_i^{*'''}(z(j))_{j,j-1} - \frac{1}{E} \mathbf{J}_i^{-1} \mathbf{f}_i^*(z(j)) \quad (30)$$

where  $j$  is the number of the considered floor, and the subscript  $j, j \pm 1$  represents the range of validity of the function. The boundary conditions for the subsequent steps are

$$\begin{aligned} \delta_i^{*''}(0) &= 0 \\ \delta_i^{*'}(H) &= 0 \\ \delta_i^*(H) &= 0 \end{aligned} \quad (31)$$

where  $z=0$  corresponds to the free-end of the bracing, and  $z=H$  is the clamped end. The corresponding conditions of continuity are given by the following expressions

$$\begin{aligned} \delta_i^{*''}(z(j))_{j,j-1} &= \delta_i^{*''}(z(j))_{j,j+1} \\ \delta_i^{*'}(z(j))_{j,j-1} &= \delta_i^{*'}(z(j))_{j,j+1} \\ \delta_i^*(z(j))_{j,j-1} &= \delta_i^*(z(j))_{j,j+1} \end{aligned} \quad (32)$$

As a result of the integration process, we obtain the relation between the displacements at each floor level  $\delta_i^*$  and the applied concentrated loads  $\mathbf{f}_i^*$ . Therefore the compliance matrix  $\mathbf{D}_i$  of the  $i$ -th bracing is

$$\delta_i^* = \frac{1}{E} \bar{\mathbf{J}}_i^{-1} h_f^3 \bar{\mathbf{Q}} \mathbf{f}_i^* = \mathbf{D}_i \mathbf{f}_i^* \quad (33)$$

where the matrix  $\bar{\mathbf{Q}}$  is a  $3N \times 3N$ -matrix of non-dimensional coefficients of influence determined by integration, and  $h_f$  is the storey height. Its structure is block diagonal, with three equal (full) submatrices  $\mathbf{Q}$

$$\bar{\mathbf{Q}} = \begin{bmatrix} \mathbf{Q} & \mathbf{0} & \mathbf{0} \\ \mathbf{0} & \mathbf{Q} & \mathbf{0} \\ \mathbf{0} & \mathbf{0} & \mathbf{Q} \end{bmatrix} \quad (34)$$

In the case of a bracing with constant cross-section, the computation of the terms of the upper triangular part of the  $N \times N$  sub-matrix  $\mathbf{Q}$  provides the generic term

$$q_{ij} = \frac{1}{6} (N-j+1)^2 (2N+j-3i+2) \quad (35)$$

The lower triangular part is obtained exploiting the symmetry of  $\mathbf{Q}$ . In the case of bracings with variable cross-section, the computation can be performed by means of the Mohr's theorem. It is worth noting that  $\delta_i^*$  and  $\mathbf{f}_i^*$  in Eq. (33) are now  $3 \times N$  vectors containing the displacements and the loads at each floor level, ordered according to the general approach presented in the previous section.  $\bar{\mathbf{J}}_i$  is a  $3N \times 3N$ -matrix with nine diagonal submatrices containing the cross-section inertia parameters

$$\bar{\mathbf{J}}_i = \begin{bmatrix} \mathbf{J}_{yy} & \mathbf{J}_{yx} & \mathbf{J}_{y\omega} \\ \mathbf{J}_{xy} & \mathbf{J}_{xx} & \mathbf{J}_{x\omega} \\ \mathbf{J}_{\omega y} & \mathbf{J}_{\omega x} & \mathbf{J}_{\omega\omega} \end{bmatrix} \quad (36)$$

By inverting the compliance matrix  $\mathbf{D}_i$ , we finally get the expression of the stiffness matrix  $\mathbf{K}_i^*$  in the local system of the  $i$ -th bracing with open thin-walled cross-section

$$\mathbf{K}_i^* = (\mathbf{D}_i)^{-1} = \frac{E}{h_f^3} \bar{\mathbf{Q}}^{-1} \bar{\mathbf{J}}_i \quad (37)$$

that, introduced in Eq. (10), permits bracings with open thin-walled cross-sections to be considered in the general formulation proposed by Carpinteri and Carpinteri (1985).

#### 4. Interaction between bracings with closed and open thin-walled cross-sections

A numerical example, chosen to show the flexibility and effectiveness of the proposed approach, is presented in this section. The structure is an asymmetric 80-storey tube-in-tube system with

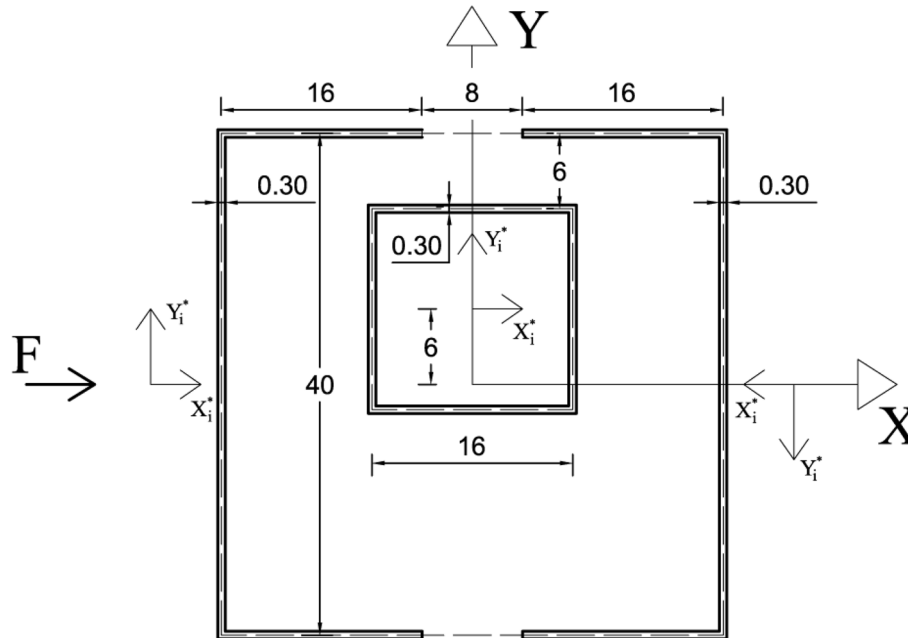


Fig. 5 Floor plane of the example building. Tube-in-tube structure with asymmetric core

Table 1 Cross-section properties for the closed thin-walled core and the external open bracings.  $J_{xx}$  and  $J_{yy}$  are referred to the barycentre,  $J_{\omega\omega}$  to the shear centre

	Core	'C'-shaped bracings
Second moment $J_{xx}$ [m <sup>4</sup> ]	819.50	5440.00
Second moment $J_{yy}$ [m <sup>4</sup> ]	819.50	550.00
Warping moment $J_{\omega\omega}$ [m <sup>6</sup> ]	0.00	154202.40
Torsional rigidity (à la de Saint Venant [m <sup>4</sup> ])	1228.80	0.65
Global coordinate $x_G$ of the shear centre [m]	0.00	± 25.65
Global coordinate $y_G$ of the shear centre [m]	-6.00	0.00
Angle $\varphi$ [rad]	0.00	0.00; 3.14

square plane layout. The asymmetry is chosen in order to investigate both the flexural and the torsional behaviour of the building when subjected to horizontal wind loads. As shown in Fig. 5, the internal core is closed, whereas the external tube is made by two bracings with 'C'-shaped open cross-sections. The Young's modulus is  $E = 3.0 \times 10^4$  MPa, the Poisson ratio  $\nu = 0.18$ . The storey height is  $h_f = 4.0$  m, corresponding to a total height  $H = 320$  m. The geometric parameters of the cross-sections are given in Table 1. The second order and sectorial moments of inertia are referred to the principal axes.

Concerning the loads, in this example we consider the actions of wind only. For the sake of simplicity, we assume constant wind pressure over the height of the structure. Due to the hypothesis of infinite rigidity of the floors in their plane, the wind actions can be applied as a system of

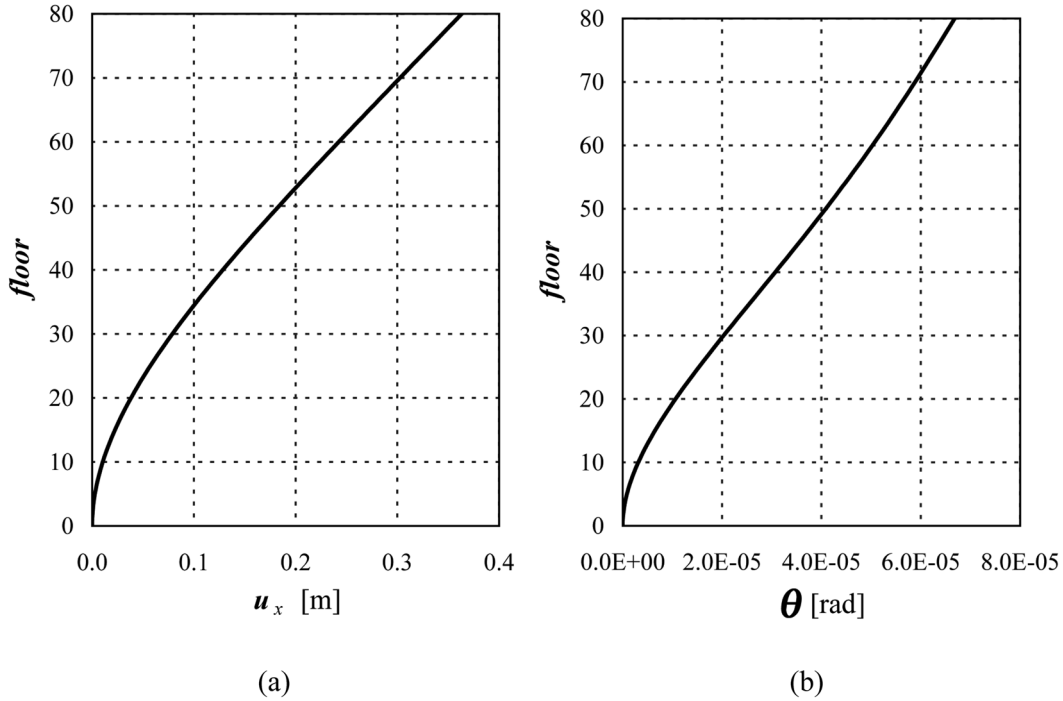


Fig. 6 Displacements of the floors in the global coordinate system. Translation in (a) the X-direction; and (b) rotation

concentrated horizontal loads passing through the barycentre of the pressure distribution. The intensity of wind actions is computed in a simplified way by considering the reference kinetic pressure provided by the Italian Technical Regulations (Ministero delle Infrastrutture 2008), that adopt the same models of wind actions contained in the Eurocode 1 (European Committee for Standardization 2002), in which the wind actions are supposed to be static and directed according to the principal axes of the structure. According to the Eurocode 1, the reference kinetic pressure is a function of the wind velocity  $v_{ref}$

$$q_{ref} = \frac{v_{ref}^2}{1.6} 10^{-3} [\text{kN/m}^2] \quad (38)$$

The reference velocity of wind is, in turn, a function of the region and of the altitude; in this example we suppose that the building is located in Turin (Piedmont, Italy). From the regulations we get  $v_{ref} = 25.0$  m/s and therefore  $q_{ref} = 390.62$  N/m<sup>2</sup>. For the sake of simplicity, we do not consider the exposition-, shape- and dynamic-coefficients (European Committee for Standardization 2002), that vary depending on several parameters (roughness, shape of the building, topography, etc). The obtained concentrated loads have the following values:  $F = 62.50$  kN, except at the top floor of the building, where the load is halved. In the computations, the wind force is applied in the X-direction only.

The results are summarized in Figs. 6 and 7. In Fig. 6(a) and (b) displacements in the X-direction and rotations at the floor levels are reported respectively; as can be seen, the flexural deformed shape does not display any change in the curvature, whereas rotations do. An inflection point is

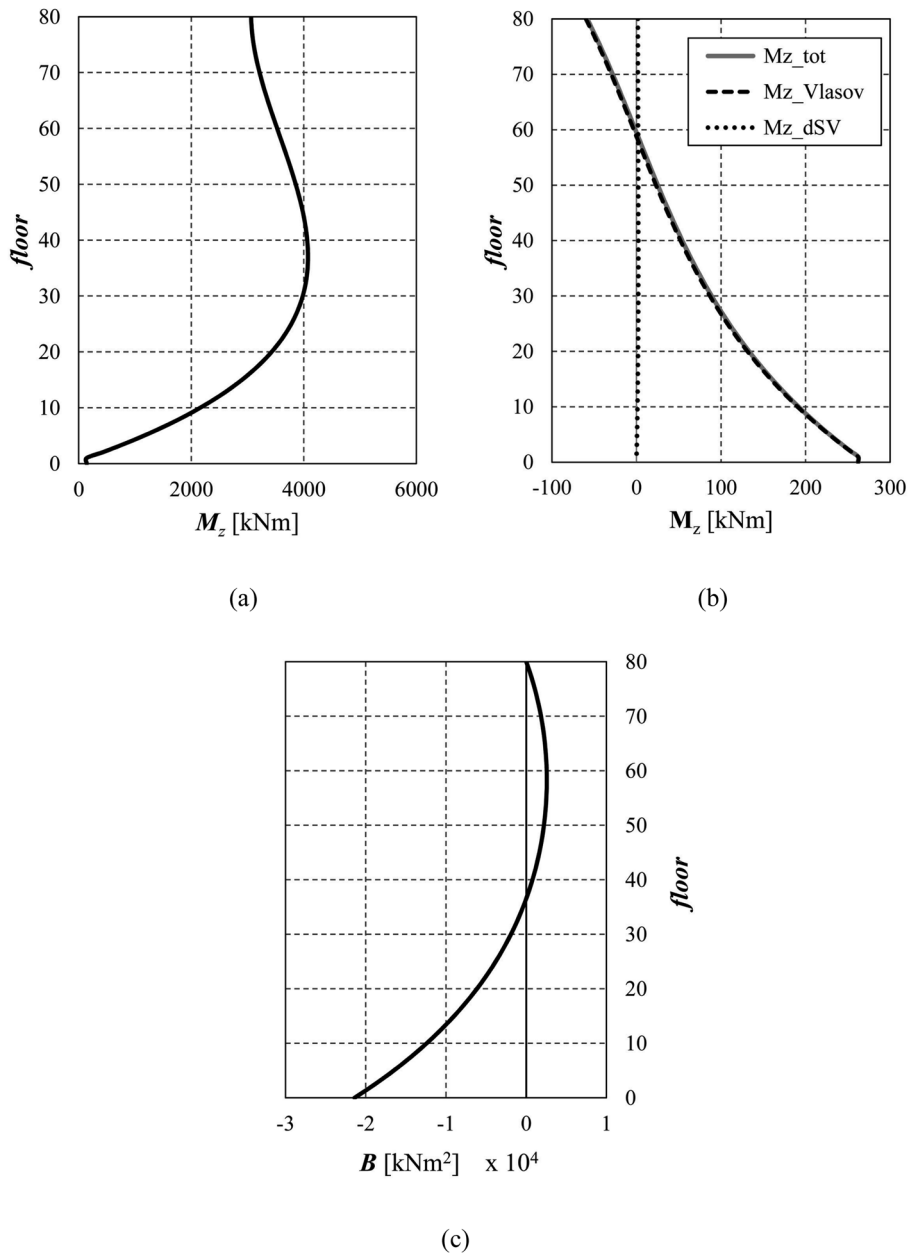


Fig. 7 (a) Torsion of the internal core; and (b) torsion and (c) bimoment of the external ‘C’-shaped bracings along the building height

clearly visible at the level of floor 37 in Fig. 6(b). This fact is in tight connection with the diagrams of the torsional moment  $M_z$ , reported in Fig. 7(a) and (b) for the internal core and the external ‘C’-shaped bracings, respectively. Regarding the internal closed core, it can be clearly seen that the torsional moment, related to de Saint Venant theory, displays a maximum at the level of floor 37

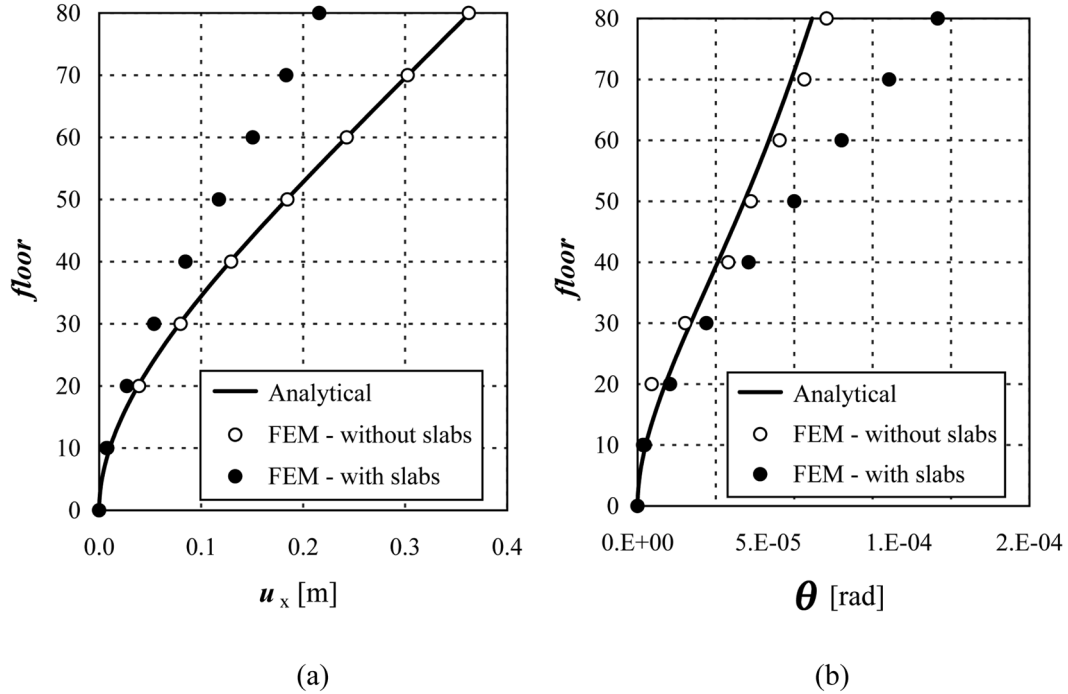


Fig. 8 Comparison between the results of the analytical method and FE solution. (a) Translation in the X-direction and (b) torsional rotation, in the global coordinate system

and decreases below. It supports a larger part of the total moment and presents null warping moment  $M_\omega$ . On the other hand, the 'C'-shaped cross-sections display a negligible primary moment and a large warping moment  $M_\omega$ . The latter changes its sign from the top of the building (where it is negative) to the ground and shows a faster rate of increase below the floor 37. The primary moment is negligible with respect to the warping one in the external bracings. All this can be confirmed if we look at the bimoment  $B$  in the external 'C'-shaped bracings (plotted in Fig. 7(c)): we can see that the sign changes at the level of floor 37, being positive above it. Correspondingly, the rotation diagram in Fig. 6(b) shows an inflection point at the same level, according to the relationship between the bimoment and the second derivative of the rotation, expressed in Eq. (22). As expected, the maximum value of the bimoment is at the ground floor, where the warping is completely prevented, and is null at the top of the building. The longitudinal stresses generated by the warping torsion, are evaluated by means of the following expression

$$\sigma_z = \frac{B\omega}{J_{\omega\omega}} \quad (39)$$

where  $\omega$  is the sectorial area.

The results of the analytical method are compared to those obtained with a FE analysis, where the bracings are modelled by two-dimensional thin shell elements. As shown in Fig. 8, the two solutions are coincident when the out-of-plane rigidity of the floor is negligible (slab thickness equal to 1/20 of the wall thickness). Considering displacements in the X-direction and using thicker floors

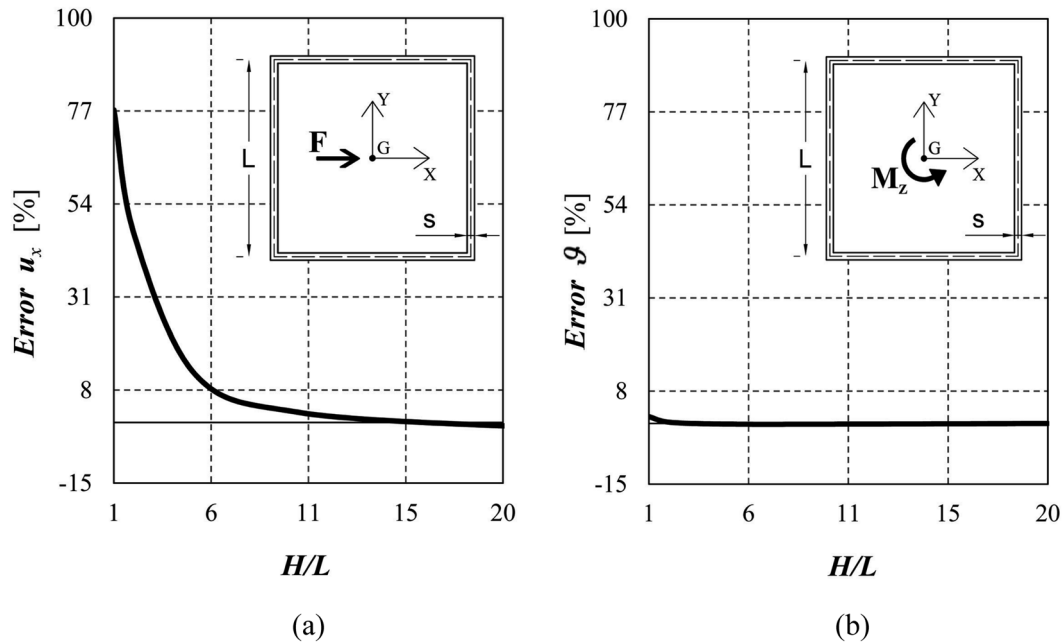


Fig. 9 Relative error for the top displacement in (a) X-direction and (b) the rotation, between the proposed method and FE analysis, for bracings of total height  $H$ , with closed cross-section

(slab thickness equal to 1/2 of the wall thickness), the FE solution is clearly stiffer than the analytical one (Fig. 8(a)). As regards the floor rotations, the FE model with out-of-plane rigid slabs shows more twist (Fig. 8(b)). This latter behaviour is caused by the warping of the external ‘C’-shaped bracings, which forces the closed section to warp significantly.

The accuracy of the proposed method has been further investigated by considering different structural arrangements and geometrical and stiffness characteristics. First, a single thin-walled cantilever beam of total height  $H$ , having closed square cross-section with side  $L$  and thickness  $s$ , is considered. The investigated variables are the overall slenderness, defined by the ratio  $H/L$ , and the cross-section slenderness, defined as  $s/L$ . The comparisons are carried out in terms of displacements of the top floor (horizontal displacement and torsional rotation). The results for horizontal forces and torsional moments applied to the barycentre of each floor are shown in Fig. 9. The relative error is defined as  $(\delta_{FE} - \delta_{an})/\delta_{FE}$ , where the pedex ‘an’ stands for ‘analytical method’. In the case of horizontal loads (Fig. 9(a)), the relative error is about 80% for very stocky bracings, due to the large shear deformations disregarded by the analytical model, whereas it decreases up to zero for very slender bracings. The same results are obtained for the three considered values of  $s/L$  (1:100, 1:50 and 1:20). In the case of torsional moments, the relative error is below 4% for any considered slenderness ratio.

The same analyses have been carried out for a cantilever beam with ‘C’-shaped thin-walled cross-section (Fig. 10). In this case, the relative error rapidly decreases for  $H/L$  varying from 1 to 7, and then it remains close to zero, for both horizontal loads and torsional moments. Also in this case, the cross-section slenderness ratio has a limited influence on the comparison.



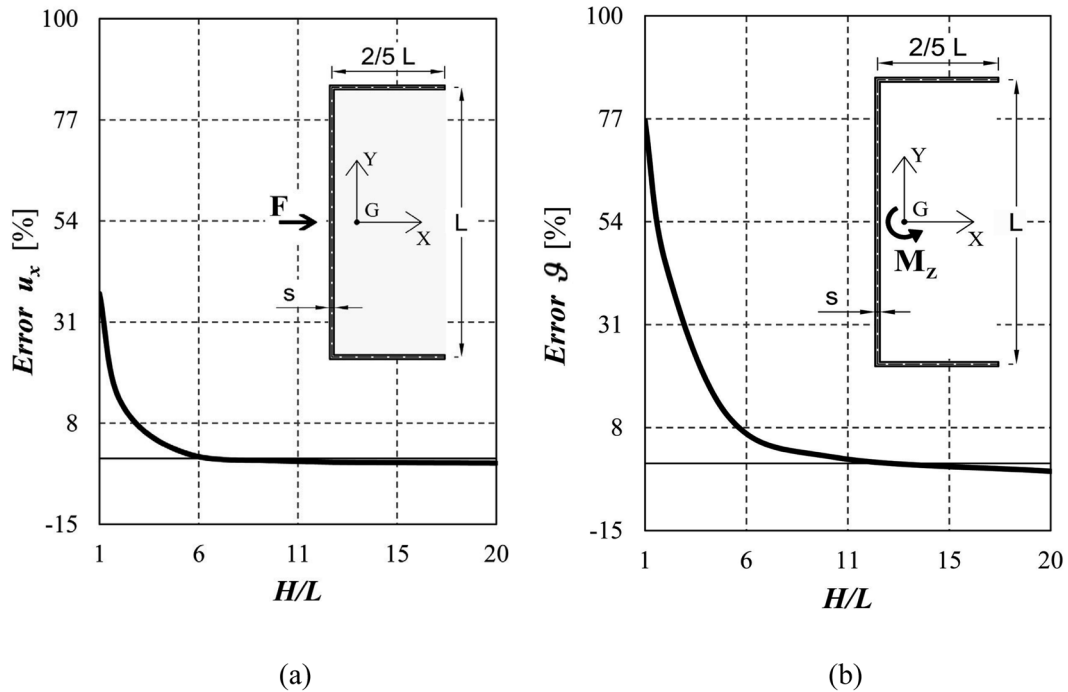


Fig. 10 Relative error for the top displacement in (a) X-direction and (b) the rotation, between the proposed method and FE analysis, for bracings of total height  $H$ , with open cross-section

## 5. Effects of bracings of different height

In this section, the interaction between bracings with different height is investigated on a structure characterised by a symmetric plan and an abrupt change in the cross-sectional geometry along the height, as shown in Fig. 11. In particular, the external stability walls have a reduced height relative to the rest of the building. In this case, the external load is constituted by a system of concentrated horizontal forces passing through the barycentre of the floor stiffness. For the sake of simplicity, a value of 1 kN is assumed for each of the forces. Such a simple structural scheme permits to analyse in a clear way the effects of the different height of bracings on the redistribution of the shear force and the bending moment.

The Young's modulus is  $E = 3.0 \times 10^4$  MPa, and the Poisson ratio  $\nu = 0.18$ . The maximum height of the building is 160 m, being the number of storeys 40 and the storey height  $h_f = 4$  m. The height of the lower part is assumed half the total height, equal to 80 m. All the bracings have the same flexural stiffness,  $EJ_{yy}$ . The storey elements, which connect the bracings each other, are modelled to be undeformable in their plane; whereas they have a negligible out-of-plane rigidity.

The most interesting result concerns the shear force distribution. A strong discontinuity with a cuspidal point at the top level of the lower bracing is evidenced when different heights are considered (see Fig. 12(a)). Such a jump in the shear distribution is due to the assumption of floor slabs undeformable in their planes. This phenomenon, also confirmed by finite element analysis, has not been noticed by the analysis carried out by Steenbergen and Blaauwendraad (2007) on a structure similar to that considered in this study, whom results are reported in Fig. 12b. On the other

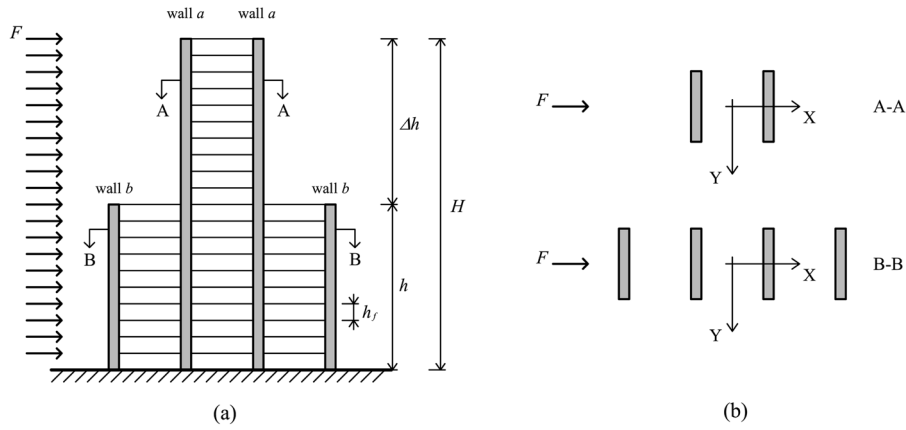
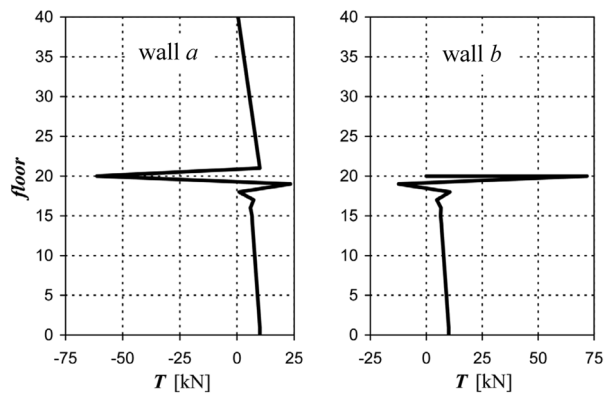
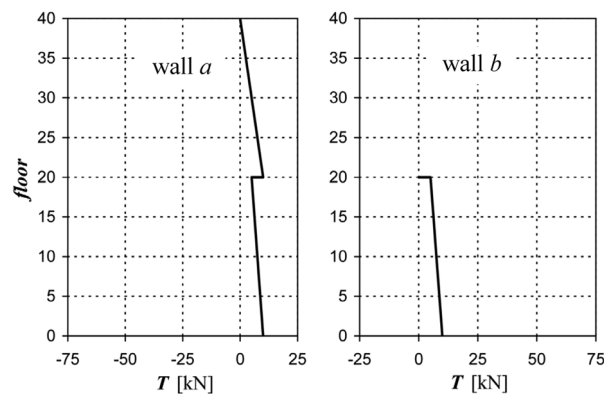


Fig. 11 (a) Front view and (b) plans of the symmetric structure with bracings of different height

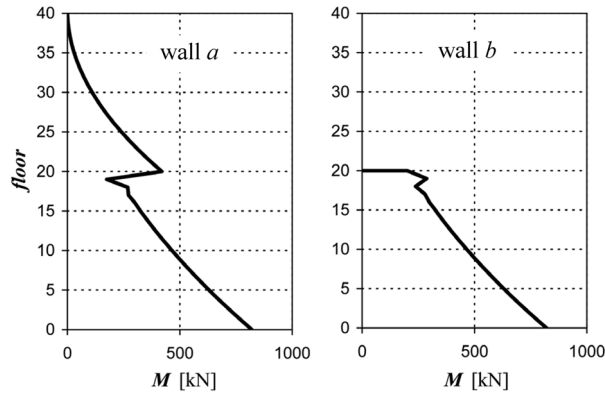


(a)

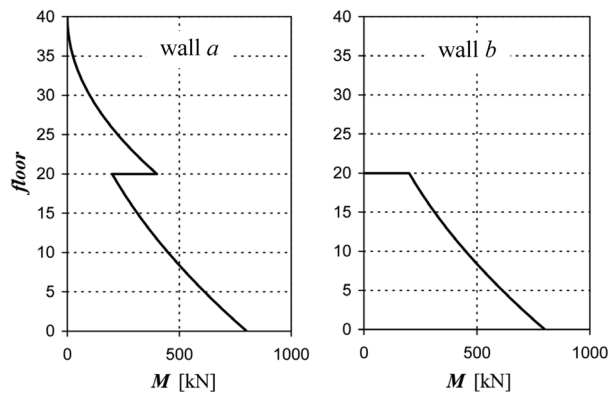


(b)

Fig. 12 Shear load distributions along the stability walls: (a) proposed model, (b) solution by Steenberg and Blaauwendraad (2007)



(a)



(b)

Fig. 13 Moment distributions along the stability walls: (a) the proposed model, (b) solution by Steenbergen and Blaauwendraad (2007)

hand, Steenbergen and Blaauwendraad (2007) demonstrated that such a discontinuity becomes smoother by decreasing the in-plane floor rigidity. The results shown in Fig. 13 highlight that also the bending moment redistributions are characterized by a discontinuity. In particular, the bending moment acting at the level of the abrupt change in the cross-sectional geometry (floor 20 in the considered case) is split proportionally to the bracing stiffness, independently of the difference in height. Also in this case, according to the study by Steenbergen and Blaauwendraad (2007), we can assert that such a discontinuity is proportional to the in-plane floor stiffness.

A reduction in the shear force exchanged by bracings at the top level of the lower wall can be obtained by varying their relative stiffness. To this aim, we define the stiffness ratio,  $SR$ , as the ratio between the stiffness of the higher and the lower bracing,  $(EJ)_H/(EJ)_L$ . The results for  $SR$  equal to 1, 10 and 100, and  $\Delta h/H$  equal to 0.5 ( $\Delta h$  and  $H$  are defined in Fig. 11), are shown in Fig. 14 in term of shear force. It is evident that the peak in the shear force distribution considerably decreases by

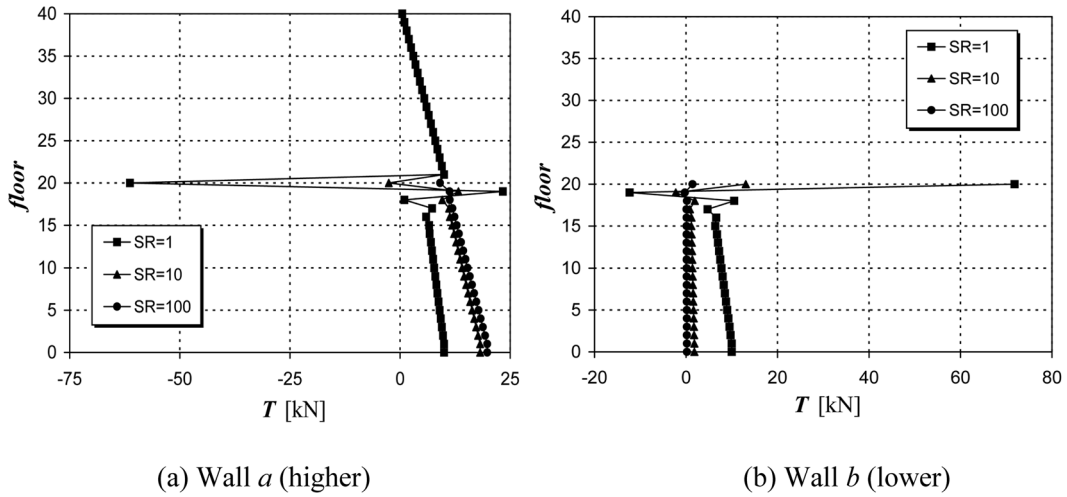


Fig. 14 Shear force distributions along bracings with difference in height equal to 50%, for three different stiffness ratios,  $SR = 1, 10, 100$

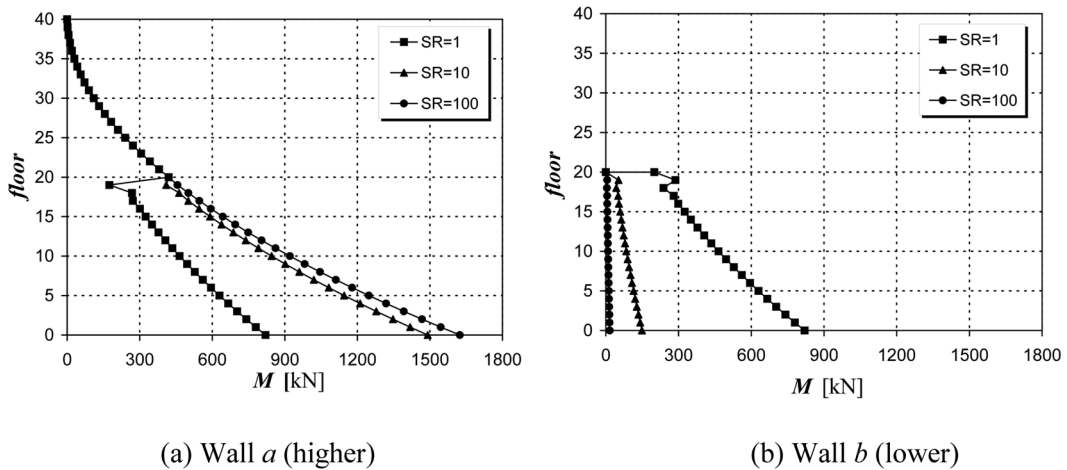


Fig. 15 Bending moment distributions along bracings with difference in height equal to 50%, for three different stiffness ratios,  $SR$

decreasing the stiffness of the lower bracing. This is due to the decrease in the support effect that the lower wall exerts to the higher. On the other hand, the contribution of the outer walls to the total load carrying capacity decreases by increasing  $SR$ . Such an effect can be also deduced from the bending moment redistribution diagrams shown in Fig. 15.

Now, the shear forces  $T_{\max}$  and  $T_{\text{ground}}$  are defined, respectively, as the shear force taking place in the considered bracing at the level of the change in the cross-sectional geometry, and that acting at the ground level. The ratio  $T_{\max}/T_{\text{ground}}$  as a function of the difference in height among the considered bracings is plotted in Fig. 16(a) for the higher walls. In the case of  $SR = 1$ , the ratio  $T_{\max}/T_{\text{ground}}$  sensibly increases by increasing  $\Delta h/H$ . In particular, for differences in height greater than

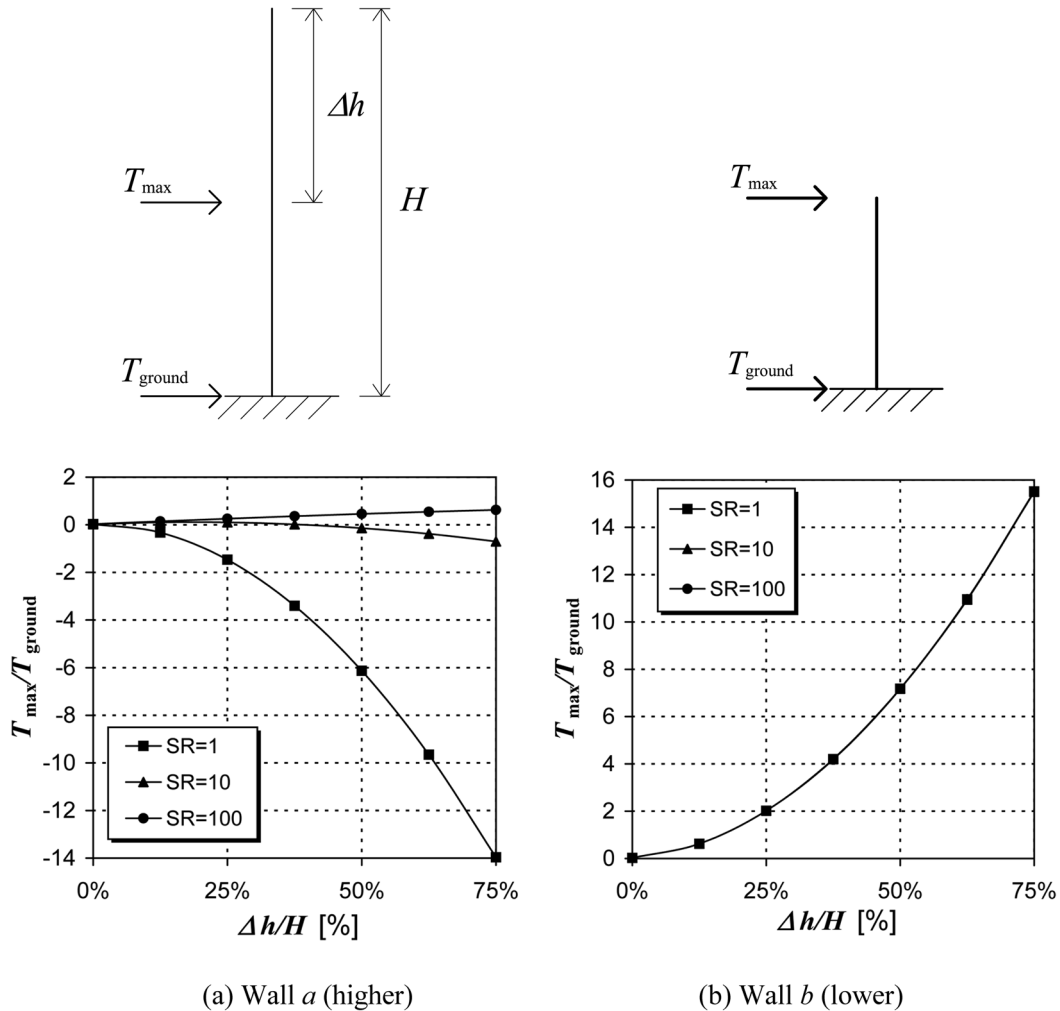


Fig. 16 Ratio between maximum and ground shear force vs. the difference in height among bracings, for three different stiffness ratios,  $SR$

20%, the ratio overcomes the unity, proving that the maximum shear force takes place at the level of the abrupt change in the cross-sectional geometry instead of at the ground level, as usually expected. On the contrary, for  $SR$  between 10 and 100, the ratio  $T_{max}/T_{ground}$  is always lower than 1. The same results are shown in Fig. 16b for the lowest wall. In this case, for  $\Delta h/H$  greater than 15%, the maximum value of the shear force is acting at the top of the bracing, independently of the ratio  $SR$ . It is worth noting that the total shear force at the ground level is shared between bracings proportionally to their flexural stiffness, independently of the height of each bracing.

Finally, some interesting remarks can be drawn considering more than one change in the cross-sectional geometry along the building height. To this aim, the four structures shown in Fig. 17(a) are considered. They are characterised by the same total flexural stiffness at the ground level, the same total height, and a different number of bracings: case “A” with two bracings, “B” with three

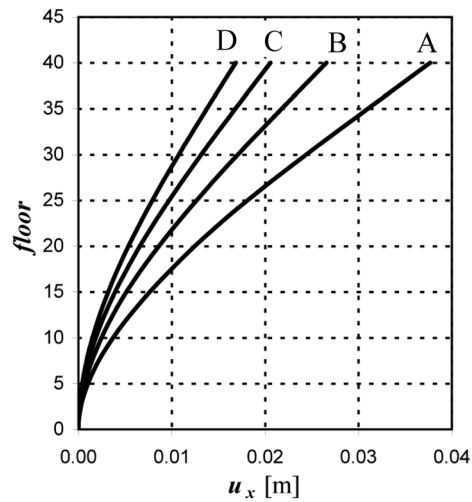
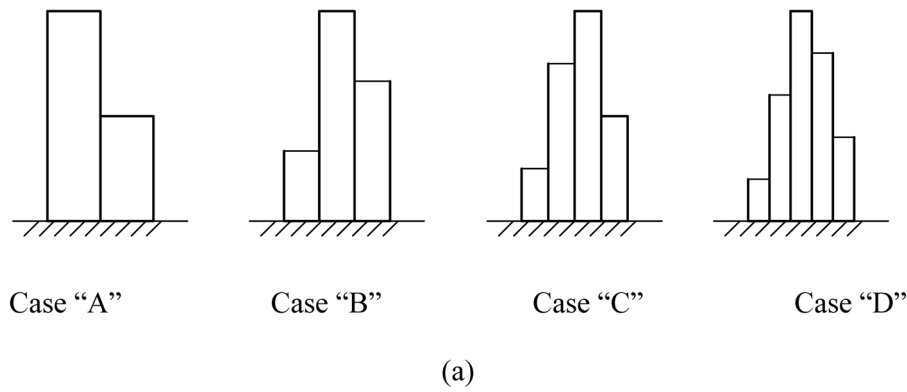
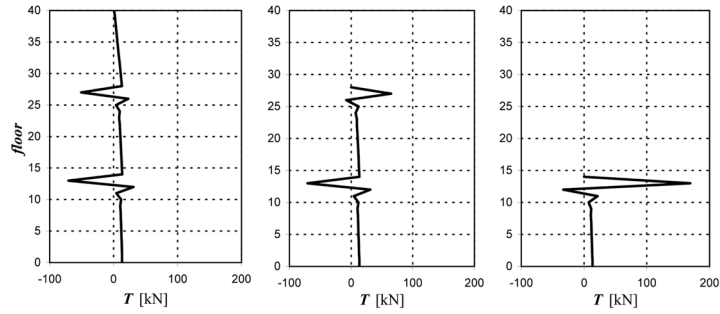
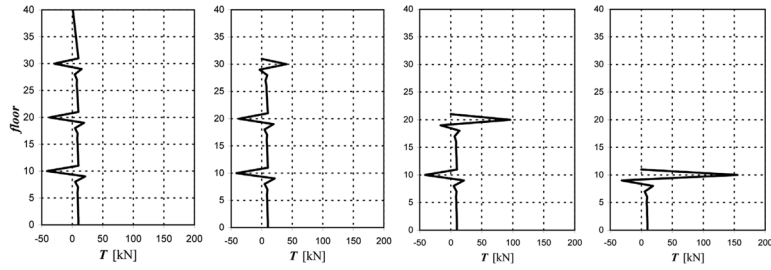


Fig. 17 (a) Structures with different changes of cross-sectional geometry; and (b) the corresponding lateral displacements

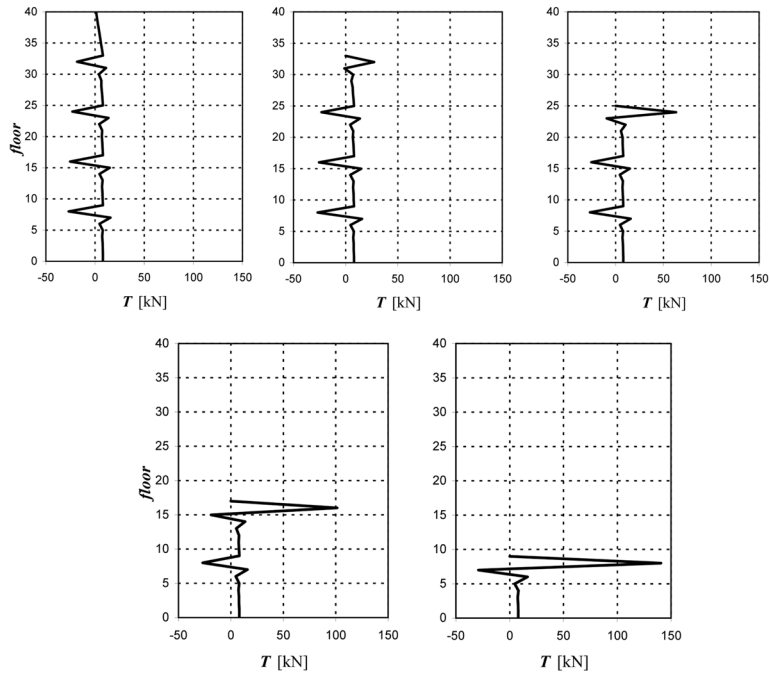
bracings, “C” with four bracings, and “D” with five bracings. For each case, the walls have the same flexural stiffness,  $EJ$ , and their heights are selected so to have a uniform  $\Delta h$ . The external load is constituted by a system of concentrated horizontal forces equal to 1 kN. The lateral floor displacements shown in Fig. 17(b) evidence a greater global stiffness in the case “D”, characterised by five changes along the height. The shear force distributions are shown in Fig. 18, except for the case “A”, whose diagrams are shown in Fig. 12(a). As we can see, the shear force at the ground level is a function only of the flexural stiffness,  $EJ$ , and not of the height. In all the considered cases, in fact, the total ground shear force is equally distributed between bracings. Then, the peaks in the shear force distributions due to the abrupt changes in the geometry, increase by decreasing the wall height, being the maximum at the top of the lower one. As a consequence, the most stressed bracing results to be the lowest.



Case "B"



Case "C"



Case "D"

Fig. 18 Shear force distributions between bracings for the considered structures: "B", "C", and "D"

## 6. Conclusions

The numerical algorithm for the lateral loading distribution between the elements of a three dimensional civil structure (Carpinteri and Carpinteri 1985), extended in this paper by introducing thin-walled elements with open cross-section and bracings of different height, can be employed to predict the gross structural deformations of tall buildings with different structural typologies. The general formulation presented in this paper offers, compared to a detailed FE simulation, ease of use and reduced effort in preparing the model, as well as in the result interpretation, with sufficient accuracy in the preliminary and conceptual design stage. In particular, such a global approach has been found to provide a reliable picture of the key structural parameters governing the building behaviour in the case of sufficiently slender bracings and floor slabs with negligible out-of-plane rigidity. The examples presented in this paper, in fact, demonstrate the flexibility and effectiveness of the proposed approach to study complex problems characterising the structural analysis. The first example concerns the lateral loading distribution in tall buildings supported by bracings with closed and open thin-walled cross-section, obeying to the Timoshenko-Vlasov torsion theory. In the second example, taking the work by Steenbergen and Blaauwendraad (2007) as the starting point, the force distribution in a structure with irregular shape, i.e., supported by bracings with different height and stiffness, is analysed.

Since modern tall buildings might take any shape and can reach huge heights with a minimum of material according to new construction techniques, the proposed algorithm is a suitable tool to face the problems resulting from the analysis of such non-conventional structures modelled as slender cantilever beams.

## Acknowledgements

The financial support provided by the Ministry of University and Scientific Research (MIUR) for the PhD scholarship "Tall buildings constructed with advanced materials: a global approach for the analysis under static and dynamic loads", is gratefully acknowledged.

## References

- Beck, H., König, G. and Reeh, H. (1968), "Kenngrößen zur Beurteilung der Torsionssteifigkeit von Hochhäusern", *Beton und Stahlbetonbau*, **63**, 268-277. (in German)
- Beck, H. and Schäfer, H.G. (1969), "Die Berechnung von Hochhäusern durch Zusammenfassung aller aussteifenden Bauteile zu einen Balken", *Der Bauingenieur*, **44**, 80-87. (in German)
- Capurso, M. (1981), "Sul calcolo dei sistemi spaziali di controventamento, parte I", *Giornale del Genio Civile*, **1-2-3**, 27-42. (in Italian)
- Carpinteri, A. and Carpinteri, An. (1985), "Lateral loading distribution between the elements of a three-dimensional civil structure", *Comput. Struct.*, **21**, 563-580.
- Carpinteri, A., Lacidogna, G. and Puzzi, S. (2010), "A global approach for three-dimensional analysis of tall buildings", *Struct. Design Tall Spec. Build.*, **19**, 518-536.
- Coull, A. and Irwin, A.W. (1972), "Model investigation of shear wall structures", *J. Struct. Div. ASCE*, **98**, 233-1237.
- Coull, A. and Bose, B. (1977), "Simplified analysis of framed-tube structures", *J. Struct. Div. ASCE*, **101**, 2223-2240.



- European Committee for Standardization (2002), *Eurocode 1: Actions on structures. General actions. Densities, self-weight, imposed loads for buildings, BS EN 1991-1-1:2002*, British Standard Institution.
- Fischer, C. and Kasal, B. (2009), "Analysis of light-frame, low-rise buildings under simulated lateral wind loads", *Wind Struct.*, **12**(2), 22-33.
- Gluck, J. and Krauss, M. (1973), "Stress analysis of group of interconnected thin-walled cantilevers", *J. Struct. Div. ASCE*, **99**, 2143-2165.
- Heidebrecht, A.C. and Stafford Smith, B. (1973), "Approximate analysis of tall wall-frame structures", *J. Struct. Div. ASCE*, **99**, 199-221.
- Hoenderkamp, J.C.D. and Snijder, H. (2000), "Approximate analysis of high-rise frames with flexible connections", *Struct. Design Tall Build.*, **9**, 233-248.
- Howson, W.P. (2006), "Global Analysis: Back to the Future", *Struct. Eng.*, **84**, 18-21.
- Humar, J.L. and Khandoker, J.U. (1980), "A computer program for three-dimensional analysis of buildings", *Comput. Struct.*, **1**, 369-387.
- Khan, F.R. (1974), "Tubular structures for tall buildings", *Handbook of Concrete Engineering*, Van Nostrand Reinhold Co., 345-355.
- Khan, F.R. and Sbarounis, J.A. (1964), "Interaction of shear walls and frames", *J. Struct. Div. ASCE*, **90**, 285-335.
- Kim, H.S. and Lee, D.G. (2003), "Analysis of shear wall with openings using super elements", *Eng. Struct.*, **25**, 981-991.
- Lee, J., Bang, M. and Kim, J.Y. (2008), "An analytical model for high-rise wall-frame structures with outriggers", *Struct. Design Tall Spec. Build.*, **17**(4), 839-851.
- Leung, A.Y.T. (1985), "Microcomputer analysis of three-dimensional tall buildings", *Comput. Struct.*, **21**, 639-661.
- Leung, A.Y.T. and Wong, S.C. (1988), "Local-global distribution factors method for tall building frames", *Comput. Struct.*, **29**, 497-502.
- Ministero delle Infrastrutture (2008), *DM 14/01/2008: Nuove norme tecniche per le costruzioni*, Gazzetta Ufficiale 04.02.2008, No. 29. (in Italian)
- Mortelmans, F.K.E.C., de Roeck, G.P.J.M. and van Gemert, D.A. (1981), "Approximate method for lateral load analysis of high-rise buildings", *J. Struct. Div. ASCE*, **107**, 1589-1610.
- Pekau, O., Zielinski, Z.A. and Lin, L. (1995), "Displacements and frequencies of tall building structures by finite story method", *Comput. Struct.*, **54**, 1-13.
- Pekau, O., Lin, L. and Zielinski, Z.A. (1996), "Static and dynamic analysis of tall tube-in-tube structures by finite story method", *Eng. Struct.*, **18**, 515-527.
- Rosman, R. (1964), "Approximate analysis of shear walls subjected to lateral loads", *ACI J.*, **21**, 717-732.
- Rosman, R. (1965), "Analysis of pierced shear walls", *Wilhelm Ernst and Sohn*, 1-64.
- Rosman, R. (1966), "Torsion of perforated concrete shafts", *J. Struct. Div. ASCE*, **95**, 991-1010.
- Rutenberg, A. and Heidebrecht, A.C. (1975), "Approximate analysis of asymmetric wallframe structures", *Build. Sci.*, **10**, 27-35.
- Stafford, S.B. and Coull, A. (1991), *Tall Building Structures: Analysis and Design*, Wiley, New York.
- Stamato, M.C. and Mancini, E. (1973), "Three-dimensional interaction of walls and frames", *J. Struct. Eng.*, **99**, 2375-2390.
- Steenbergen, R.D.J.M. and Blaauwendraad, J. (2007), "Closed-form super element method for tall buildings of irregular geometry", *Int. J. Solids Struct.*, **44**, 5576-5597.
- Taranath, S.B. (1988), *Structural Analysis and Design of Tall Buildings*, McGraw-Hill, New York.
- Taranath, S.B. (2005), *Wind and Earthquake Resistant Buildings*, Marcel Dekker, New York.
- Timoshenko, S. (1936), *Theory of Elastic Stability*, (First Edition), McGraw-Hill Book Company inc., New York.
- Vlasov, V. (1961), *Thin-Walled Elastic Beams*, (Second Edition), (Jerusalem: Israeli Program for scientific translation), US Science Foundation, Washington.
- Wong, C.W. and Lau, S.L. (1989), "Simplified finite element analysis of three-dimensional tall building structures", *Comput. Struct.*, **33**, 821-830.

**Notations**

- $\mathbf{A}_i$  matrix of coefficients relating the bracing internal loadings in the local system to those in the global system;
- $\mathbf{B}_i$  matrix of coefficients relating the bracing displacements in the local system to those in the global system;
- $E$  Young's modulus;
- $\mathbf{f}$  vector of external applied load, in the global coordinate system;
- $\mathbf{f}_i$  vector of internal loading transmitted to the  $i$ -th bracing, in the global system;
- $\mathbf{f}_i^*$  vector of internal loading transmitted to the  $i$ -th bracing, in the local system;
- $\mathbf{D}_i$  compliance matrix of the  $i$ -th bracing;
- $H$  total building height;
- $h_f$  storey height;
- $\mathbf{K}$  global stiffness matrix referred to the global system;
- $\mathbf{K}_i$  stiffness matrix of the  $i$ -th bracing referred to the global system;
- $\mathbf{K}_i^*$  stiffness matrix of the  $i$ -th bracing referred to the local system;
- $\mathbf{J}_i$  matrix of inertia of the  $i$ -th bracing;
- $\mathbf{m}_i^*$  vector containing the bending moments  $M_x$  and  $M_y$ , and the bimoment,  $B$ ;
- $m_z$  applied torsional moment;
- $N$  number of floors;
- $\mathbf{N}_i$  orthogonal rotation matrix;
- $p_x$  applied horizontal load, in  $x$  direction;
- $p_y$  applied horizontal load, in  $y$  direction;
- $\mathbf{T}_i$  matrix of coefficients relating the bracing displacements to the floor displacements;
- $\mathbf{t}_i^*$  vector containing the shear forces  $T_x$  and  $T_y$ , and the torsional moment,  $M_z$ ;
- $\delta$  vector of floor displacements in the global system;
- $\delta_i$  vector of displacements of the  $i$ -th bracing in the global system;
- $\delta_i^*$  vector of displacements of the  $i$ -th bracing in the local system;
- $\Delta h$  difference in height between bracings;
- $\varphi$  rotation between local and global systems;
- $\xi$  displacement in the X-direction;
- $\eta$  displacement in the Y-direction;
- $\vartheta$  rotation;
- $\psi$  coordinate-vector of the origin of the local system in the global one.